Nat. Hazards Earth Syst. Sci., 12, 2759–2768, 2012
www.nat-hazards-earth-syst-sci.net/12/2759/2012/
doi:10.5194/nhess-12-2759-2012

Natural Hazards and Earth System Sciences

Assessment of liquefaction potential index for Mumbai city

J. Dixit, D. M. Dewaikar, and R. S. Jangid

Department of Civil Engineering, Indian Institute of Technology Bombay, Mumbai-400 076, India

Correspondence to: J. Dixit (jagabandhu@iitb.ac.in)

Received: 21 October 2011 – Revised: 13 April 2012 – Accepted: 27 May 2012 – Published: 6 September 2012

Abstract. Mumbai city is the financial capital of India and is fifth most densely populated city in the world. Seismic soil liquefaction is evaluated for Mumbai city in terms of the factors of safety against liquefaction (FS) along the depths of soil profiles for different earthquakes with 2 % probability of exceedance in 50 yr using standard penetration test (SPT)-based simplified empirical procedure. This liquefaction potential is evaluated at 142 representative sites in the city using the borehole records from standard penetration tests. Liquefaction potential index (LPI) is evaluated at each borehole location from the obtained factors of safety (FS) to predict the potential of liquefaction to cause damage at the surface level at the site of interest. Spatial distribution of soil liquefaction potential is presented in the form of contour maps of LPI values. As the majority of the sites in the city are of reclaimed land, the vulnerability of liquefaction is observed to be very high at many places.

1 Introduction

Liquefactions and associated ground failures have been widely observed during numerous devastating earthquakes. Liquefaction occurs generally due to rapid loading during seismic events where there is not sufficient time for dissipation of excess pore-water pressures through natural drainage. Rapid loading situation increases pore-water pressures resulting in cyclic softening in fine-grained materials. The increased pore water pressure transforms granular materials from a solid to a liquefied state. Shear strength and stiffness of the soil deposit are reduced due to increase in pore-water pressure. Liquefaction is observed in loose, saturated, and clean to silty sands. The soil liquefaction depends on the magnitude of earthquake, intensity and duration of ground motion, the distance from the source of the earthquake, site-specific conditions, ground acceleration, type of soil and thickness of the soil deposit, relative density, grain size distribution, fines content, plasticity of fines, degree of saturation, confining pressure, permeability characteristics of soil layer, position and fluctuations of the groundwater table, reduction of effective stress, and shear modulus degradation (Youd and Perkins, 1978; Kramer, 1996; Tuttle et al., 1999; Youd et al., 2001). Liquefaction-induced ground failure is influenced by the thickness of non-liquefied and liquefied soil layers (Ishihara, 1985). Measures to mitigate the damages caused by liquefaction require accurate evaluation of liquefaction potential of soils.

The potential for liquefaction to occur at certain depth at a site is quantified in terms of the factors of safety against liquefaction (FS). Seed and Idriss (1971) proposed a simplified procedure to evaluate the liquefaction resistance of soils in terms of factors of safety (FS) by taking the ratio of capacity of a soil element to resist liquefaction to the seismic demand imposed on it. Capacity to resist liquefaction is computed as the cyclic resistance ratio (CRR), and seismic demand is computed as the cyclic stress ratio (CSR). FS of a soil layer can be calculated with the help of several in-situ tests such as standard penetration test (SPT), conic penetration test (CPT), Becker penetration test (BPT) and shear wave velocity (V_s) test (Youd et al., 2001). SPT-based simplified empirical procedure is widely used for evaluating liquefaction resistance of soils. Factors of safety (FS) along the depth of soil profile are generally evaluated using the surface level peak ground acceleration (PGA), earthquake magnitude (M_w), and SPT data, namely SPT blow counts (N), overburden pressure (σ_v), fines content (FC), clay content, liquid limits and grain size distribution (Seed and Idriss, 1971; Seed et al., 1985; Youd et al., 2001). A soil layer with $FS < 1$ is generally classified as liquefiable and with $FS > 1$ is classified as non-liquefiable (Seed and Idriss, 1971). A layer may liquefy during an earthquake, even for $FS > 1.0$. A factor of safety of 1.2 at a particular depth is considered as the threshold value

for the layer to be categorized as non-liquefiable (Sonmez, 2003). Seed and Idriss (1982) considered the soil layer with FS value between 1.25 and 1.5 as non-liquefiable. Soil layers with FS greater than 1.2 and FS between 1.0 and 1.2 are defined as non-liquefiable and marginally liquefiable layers, respectively (Ulusay and Kuru, 2004). Although FS shows the liquefaction potential of a soil layer at a particular depth in the subsurface, it does not show the degree of liquefaction severity at a liquefaction-prone site. Iwasaki et al. (1978) proposed liquefaction potential index (LPI) to overcome this limitation of FS. Liquefaction potential index (LPI) provides an integration of liquefaction potential over the depth of a soil profile and predicts the performance of the whole soil column as opposed to a single soil layer at particular depth and depends on the magnitude of the peak horizontal ground acceleration (Luna and Frost, 1998). LPI combines depth, thickness, and factor of safety against liquefaction (FS) of soil layers and predicts the potential of liquefaction to cause damage at the surface level at the site of interest. Iwasaki et al. (1982) identified that liquefaction effects are moderate for $5 < \mathrm{LPI} < 15$ and major for $\mathrm{LPI} > 15$. Toprak and Holzer (2003) reported that sand boils occur for $\mathrm{LPI} \geq 5$ and lateral spreads occur for $\mathrm{LPI} \geq 12$. Juang et al. (2005) studied the effects of liquefaction on the damage of ground surface near foundations. LPI shows a clear picture of liquefaction severity during seismic events, and $\mathrm{LPI} \geq 5$ is generally considered as a threshold for the surface manifestation of liquefaction (Iwasaki et al., 1982; Toprak and Holzer, 2003; Holzer et al., 2006). Sonmez (2003) categorized the sites with $\mathrm{LPI} = 0$ as not likely to liquefy and categorized the sites with $0 < \mathrm{LPI} < 2$, $2 < \mathrm{LPI} < 5$, $5 < \mathrm{LPI} < 15$, and $\mathrm{LPI} > 15$ as having low, moderate, high, and severe liquefaction susceptibility, respectively. İnce (2011) prepared liquefaction susceptibility microzonation map based on LPI for the earthquakes with probability of exceedance of 10 % in 50 yr. Dixit et al. (2012) computed FS values for Mumbai city for the earthquakes with return period of 475- and 2475-yr. In this article, an attempt has been made to determine the liquefaction potential index (LPI) from the factors of safety (FS) along the depth at each representative borehole at Mumbai city based on the method proposed by Youd et al. (2001).

2 The study area

Mumbai is the financial capital of India and is fifth most densely populated city in the world. This is a peninsular city situated about midway on the western coast of stable continental region of Peninsular India.

2.1 Geomorphologic and geologic setting

The city lies in the latitudes of 18°53′ N to 19°19′ N and longitudes of 72°45′ E to 73°06′ E. The total area of the city including its suburbs is 603.4 km^2. Seven islands consisting of volcanic bedrock, separated by marshy tidal flats and creeks, were merged together by reclaiming land from the Arabian Sea over a period of two centuries to form the present city. The city is separated from the mainland by the estuary in the Vasai Creek in the north, Ulhas River in the northeast, Thane Creek and the Harbour Bay in the east, and Arabian Sea to the south and to the west. The northeastern coast of the city along the Thane Creek in the east and Manori Creek in the west is covered with mangrove swamps and marshy tidal mudflats. There are several water bodies within the city range. Three major lakes within the city limits are Powai Lake, Vihar Lake and Tulsi Lake. Sanjay Gandhi National Park, within the city range, extends over an area of 103.09 km^2. The average elevation of the city is 14 m a.m.s.l. Many places in the city lie below or just above the sea level. There are many ridges within the city range. Northern part of the city is hilly. The elevations of the ridges in the city generally vary from 90 m to 110 m a.m.s.l. and the highest elevation is 450 m. A series of N–S trending low elevation hills and some tidal flats separate Trombay Island from the city. The shoreline belt comprises sandy beach, cliffs, stream deltas, creek outlets and swamps. The landform and the width of the belt vary depending on the type of rocks and sediments. Basalt outcrops at a few places appear as narrow ridges.

The city is occupied by horizontally lying Deccan black basalt flows of cretaceous–eocene age and the associated pyroclastics and the plutonic rocks of cretaceous–palaeogene age (Sethna, 1981). Outcrops of Deccan Traps at a few places reveal that the geology of the area mainly includes products of silicic volcanism and basalt subaqueous volcanism. Pyroclastic deposits are seen in the northern part of the city (Sethna and Battiwala, 1980). Rhyolites and quartz trachytes occur in the western ridges. Stratified ash beds up to a thickness of about 45 m are observed at the western ridges, and these ash beds are underlain by hard andesitic lava flows. The rock stratigraphic sequence in the region is laterite, trap dykes, volcanic agglomerate and breccia, basalt flows and stratified fossiliferous beds (Sethna, 1999). The areas at higher elevation are underlain by amygdaloidal basalt, tuffs and trachytes (Shah and Parthasarathy, 1982). Basalts interbedded with tuffs are predominant on the mainland, and basalt along with breccia and tuff are predominant in the west coast of the city. The low lying areas are underlain by weak volcanic rocks that weather rapidly.

2.2 Seismotectonic setting and seismicity

Mumbai lies in the seismically active Panvel zone (Chandra, 1977). The length of N–S trending Panvel flexure is about 150 km. There are major fault lines that lie under Thane, Panvel and Dharamtar Creeks (Subrahmanyan, 2001). Some minor fault lines also lie under Powai Lake, Vihar Lake, Tulsi Lake, Ulhas River, Malad and Manori Creeks, and near the eastern suburbs. The city has experienced several

earthquakes, such as 1967 Koyna earthquake, 1993 Latur earthquake, 1999 Jabalpur earthquake and 2001 Bhuj earthquake. The intensities ranging between VI and VII were observed in the city during 2001 Bhuj earthquake (Hough et al., 2002). As per IS 1893-part 1 (2002), the city comes under seismic zone III of moderate seismic risk.

Raghukanth and Iyengar (2006) identified the presence of 23 major faults that are very likely to influence seismic hazard in Mumbai city, and they estimated seismic hazard for the city in the form of uniform hazard response spectra (UHRS) of 475-yr and 2475-yr return period based on probabilistic seismic hazard analysis (PSHA). Mohan et al. (2007) reported the occurrence of 41 small earthquakes around Mumbai during 1998–2005. Martin and Szeliga (2010) estimated the probable return period for V, VI, and VII intensity for the city as 42, 78, and 145 yr, respectively. Mhaske and Choudhury (2010) studied soil liquefaction for Mumbai city and identified few liquefiable sites in the city for earthquakes of magnitudes $M_w = 5.0$–7.5. Dixit et al. (2011) estimated the spatial distribution of surface level free-field ground motion in Mumbai city due to multiple suites of input earthquake ground motions scaled to match uniform hazard response spectrum (UHRS) with 10 % and 2 % probability of exceedance in 50 yr. Raghukanth (2011) estimated the seismic activity rate (λ), b-value and maximum expected magnitude (M_{max}) for the 300-km control region surrounding the city as 0.32 ± 0.06, 0.82 ± 0.07, and 6.8, respectively.

2.3 Geotechnical site characteristics

The city is predominantly covered with alluvium (GSI, 2001). Many regions of the city are systematically filled with reclaimed soil. Tidal flats, estuaries and swamps are underlain by clay-rich sediments. Sandy beaches consist of clay mixed with shells. Bedrock level in the city is generally shallow (<10 m), and the thickness of the soil cover is 20–30 m in tidal creeks and swamps. Low lying coastal plains of width 5–10 km lie between the sea and the low elevation ridges. Soil cover in most hills ranges from 1–5 m. The soil stratigraphic sequence at many places in the city is alluvium, sand, recent conglomerate, weathered residual soil, weathered rock and hard bedrock. The plains to the western part of the city represent saline marine mud, limestone, calcareous sandstones, etc. The soil cover in the suburbs is mostly loamy and alluvial. Soils in the coastal plain are brown and have a sandy texture.

Most of the input parameters such as groundwater depth, SPT N values, dry density, wet density, specific gravity, and fines content (FC), required for the liquefaction potential analyses of the soil profiles at different soil sites in the city, are obtained from the SPT borehole data obtained from different sources. Most of the SPT boreholes are densely clustered in the constructed areas. A representative site is chosen from the cluster of adjacent boreholes. The borehole records from SPT tests are collected for 142 representative borehole

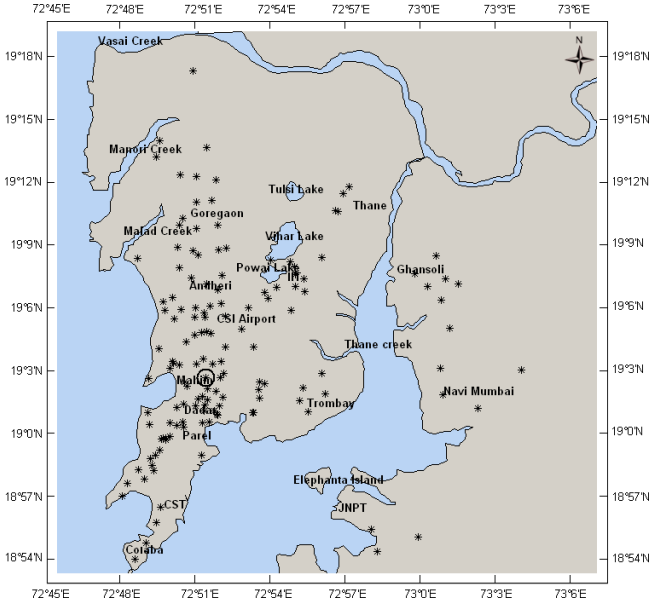

Fig. 1. Map of Mumbai city showing the borehole locations selected for liquefaction studies.

locations in the city to evaluate the liquefaction potential index (LPI). The borehole locations considered in the present study are marked as asterisks (*) in Fig. 1. The depths of boreholes are in the range of 7.0–30 m. The SPT blow counts at some places are in the order of 2–10 indicating soft deposits of clay, whereas at many of the places it is up to 40 showing dense silty sand.

Site conditions can be characterized into different categories according to the mean shear wave velocity of the upper 30 m ($\bar{V}_{s,30}$) as per the provisions in National Earthquake Hazards Reduction Program (NEHRP, 2009). The site classification system suggests that 9 sites correspond to E-type ($\bar{V}_{s,30} < 180\,m\,s^{-1}$), 94 sites correspond to D-type ($180\,m\,s^{-1} \le \bar{V}_{s,30} \le 360\,m\,s^{-1}$), and 39 to C-type sites ($360\,m\,s^{-1} \le \bar{V}_{s,30} \le 760\,m\,s^{-1}$). The majority of the sites are of D- and C-types. The spatial distribution of mean shear wave velocity ($\bar{V}_s$) at Mumbai city is presented in the form of a contour map in Fig. 2. Another approach of site classification uses characteristic site period parameter. Characteristic site period (T_s) at a site is the period of vibration corresponding to the fundamental lowest natural frequency. This parameter takes into account the effects of stiffness and density of soil, thickness of soil layers and the depth of the soil column. It can either be measured directly or can be computed as four times the travel time of the shear wave through the soil profile above bedrock. For soil sites with multiple horizontal layers, it can be computed from available geotechnical data at different sites using Eq. (1) (Kramer, 1996):

$$T_s = \sum \frac{4H_i}{V_{si}} \quad (1)$$

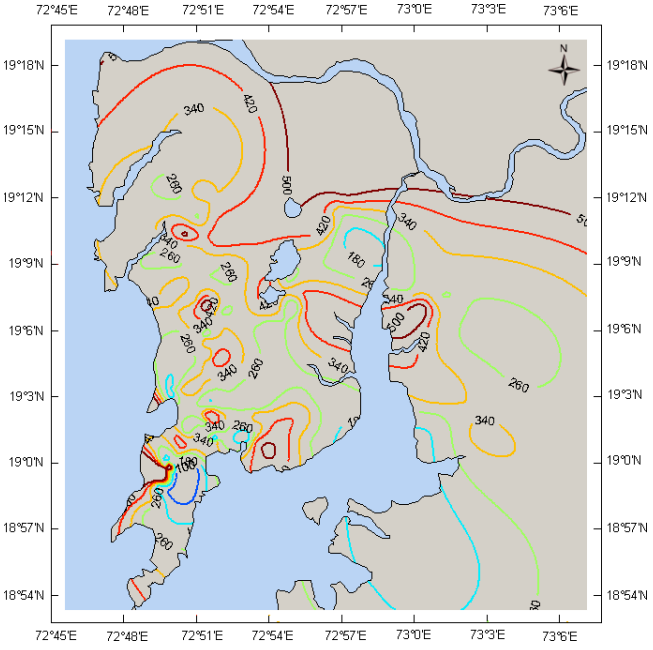

Fig. 2. Contour map of spatial distribution of mean shear wave velocity for Mumbai city.

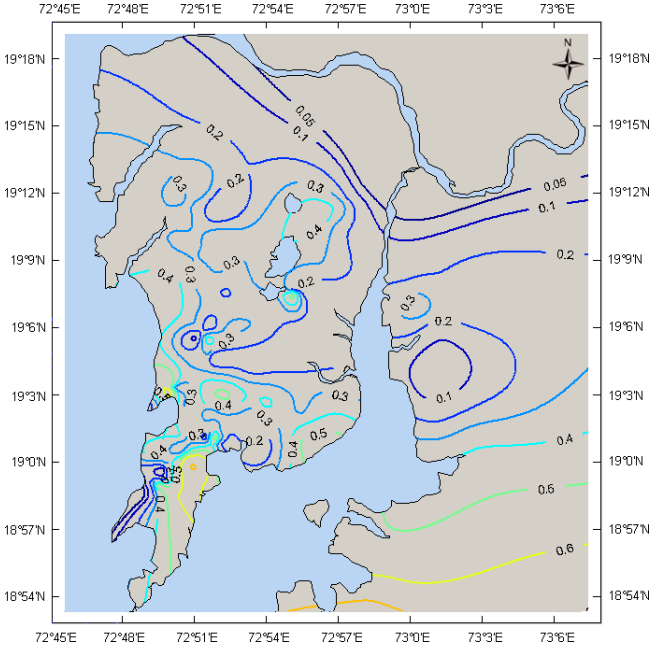

Fig. 3. Contour map of spatial distribution of site periods for Mumbai city.

where H_i is the thickness of i-th layer and V_{si} is the average shear wave velocity of i-th layer.

The spatial distribution of site period (T_s) at Mumbai city is presented in the form of a contour map in Fig. 3. T_s values also give knowledge about characteristics of different sites that influence the site response during seismic events.

In this study, seismic soil liquefaction is evaluated in terms LPI using SPT- based simplified empirical procedure. An earthquake triggered at one hypocenter is of one moment magnitude, but it produces ground motions of different PGA values at different sites depending on source characteristics, epicentral distances, effects of travel path on the seismic waves, and local site conditions. Many moderate earthquakes generate ground motions of larger PGA values than those of major earthquakes. Ground motion varies significantly over very short distances due to variation in soil type and the thickness of soil deposit (Boatwright et al., 1991). Variations in PGA of surface level ground motions due to small differences in local soil conditions and geological features between nearby sites can be high in the city, and therefore one PGA value can correspond to earthquakes of different magnitudes. Therefore, this study attempts to perform liquefaction potential analyses for earthquakes of magnitudes $M_w = 6.0$, $M_w = 6.5$ and $M_w = 7.0$ with peak horizontal ground surface acceleration (a_{max}) of 0.3 g. This a_{max} level corresponds to earthquakes of different magnitudes with 2 % probability of exceedance in 50 yr at D-type sites (Raghukanth and Iyengar, 2006). The use of this value of a_{max} is considered reasonable for the earthquakes with 2475 yr of return period, as the majority of the sites in the city belong to D-type category.

3 Assessment of liquefaction potential index

The liquefaction potential index (LPI) quantifies the severity of liquefaction and predicts surface manifestations of liquefaction, liquefaction damage or failure potential of a liquefaction-prone area (Luna and Frost, 1998). LPI is computed by taking integration of one minus the liquefaction factors of safety along the entire depth of soil column limited to the depths ranging from 0 to 20 m below the ground surface at a specific location. The level of liquefaction severity with respect to LPI as per Iwasaki et al. (1982), Luna and Frost (1998), and MERM (2003) is given in Table 1. The factors of safety against liquefaction (FS) and the corresponding liquefaction potential index (LPI) are determined by comparing the seismic demand expressed in terms of cyclic stress ratio (CSR) to the capacity of liquefaction resistance of the soil expressed in terms of cyclic resistance ratio (CRR).

3.1 Determination of cyclic stress ratio

Cyclic stress ratio (CSR) characterizes the seismic demand induced by a given earthquake, and it can be determined from peak ground surface acceleration that depends upon site-specific ground motions. The expression for CSR induced by earthquake ground motions formulated by Idriss and Boulanger (2006) is as follows:

$$\mathrm{CSR} = 0.65 \frac{a_{max}}{g} \frac{\sigma_v}{\sigma'_v} r_d \frac{1}{\mathrm{MSF}} \frac{1}{K_\sigma}. \quad (2)$$

0.65 is a weighing factor to calculate the equivalent uniform stress cycles required to generate same pore water pressure

Table 1. The level of liquefaction severity.

LPI	Iwasaki et al. (1982)	Luna and Frost (1998)	MERM (2003)
LPI = 0	Very low	Little to none	None
0 < LPI < 5	Low	Minor	Low
5 < LPI < 15	High	Moderate	Medium
15 < LPI	Very high	Major	High

during an earthquake; a_{max} is the peak horizontal ground acceleration; g is acceleration of gravity; σ_v and σ'_v are total vertical overburden stress and effective vertical overburden stress, respectively, at a given depth below the ground surface; r_d is depth-dependent stress reduction factor; MSF is the magnitude scaling factor, and K_σ is the overburden correction factor.

This stress reduction factor (r_d) accounts for the dynamic response of the soil column and represents the variation of shear stress amplitude with depth. Idriss and Boulanger (2006) formulated following expressions to calculate the stress reduction factor (r_d):

$$r_d = \exp[\alpha(z) + \beta(z) M_w] \quad (3)$$

$$\alpha(z) = -1.012 - 1.126 \sin\left(\frac{z}{11.73} + 5.133\right) \quad (4)$$

$$\beta(z) = 0.106 + 0.118 \sin\left(\frac{z}{11.28} + 5.142\right) \quad (5)$$

where z is the depth (in m) and M_w is moment magnitude. The arguments inside the sine terms in Eqs. (4) and (5) are in radians. The above expression for r_d is valid up to a depth of $z \leq 34$ m, and the depths of boreholes considered in the present analysis are less than 34 m.

The values of CSR that pertain to the equivalent uniform shear stress induced by an earthquake of magnitude, M_w, are adjusted to an equivalent CSR for an earthquake of magnitude $M_w = 7.5$ through introduction of magnitude scaling factor (MSF). MSF accounts for the duration effect of ground motions. MSF for $M_w < 7.5$ is expressed as follows:

$$\text{MSF} = 6.9 \exp\left(\frac{-M_w}{4}\right) - 0.058 \leq 1.8. \quad (6)$$

Since the liquefaction resistance increases with increasing confining stress, the overburden correction factor (K_σ) is applied such that the values of CSR are adjusted to an equivalent overburden pressure $\sigma_{v'}$ of 1 atmosphere.

$$K_\sigma = 1 - C_\sigma \ln\left(\frac{\sigma_{v'}}{p_a}\right) \leq 1.0 \quad (7)$$

where

$$C_\sigma = \frac{1}{18.9 - 2.5507\sqrt{(N_1)_{60}}} \leq 0.3 \quad (8)$$

p_a is the atmospheric pressure (= 100 kPa). The measured SPT N values (N_m) are corrected for overburden stress, energy ratio, diameter of boreholes, length of sampling rod and the type of sampler by introducing a series of correction factors. N_{60} is the corrected Nm value for 60 % energy ratio with an assumption that 60 % of the energy is transferred from the falling hammer to the SPT sampler. The corrected $(N_1)_{60}$ values are calculated as

Table 2. Rod length correction with respect the depth.

Depth, d	Correction for rod length, C_R
d < 3 m	0.75
d = 3–4 m	0.8
d = 4–6 m	0.85
d = 6–10 m	0.95
d = 10–30 m	1.0

$$(N_1)_{60} = N_m C_N C_E C_B C_R C_S \quad (9)$$

where C_N is a factor to normalize N_m to a common reference effective overburden stress; C_E is correction for hammer energy ratio (ER); C_B is correction factor for borehole diameter; C_R is correction factor for rod length; and C_S is correction for samplers with or without liners. The value of C_N is calculated as per Eq. (10) and is limited to a maximum value of 1.7. C_S, C_B, and C_E are assumed to be 1.1, 1.0, and 0.6, respectively. Rod length correction with respect the depth (C_R) at each borehole location is corrected as per Table 2, suggested by Youd et al. (2001).

The overburden correction (C_N) factor to normalize $(N_1)_{60}$ to a common reference effective overburden stress is

$$C_N = \left(\frac{p_a}{\sigma'_v}\right)^\alpha \leq 1.7 \quad (10)$$

where

$$\alpha = 0.784 - 0.0768\sqrt{(N_1)_{60}}. \quad (11)$$

It can be observed from Eqs. (10) and (11) that $(N_1)_{60}$ and C_N are interdependent. A series of iterations are carried out to determine $(N_1)_{60}$ and C_N until the difference between successive iteration values is less than 0.001.

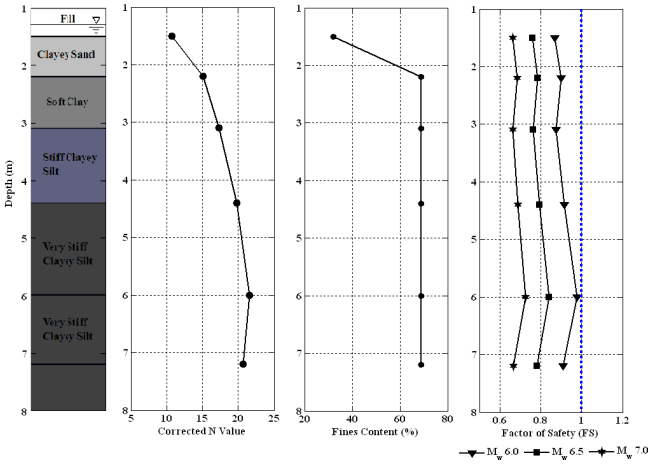

Fig. 4. Soil profile, corrected N values, fine content, FS values against liquefaction along the depth at a typical site (the site is shown as encircled * in Fig. 1).

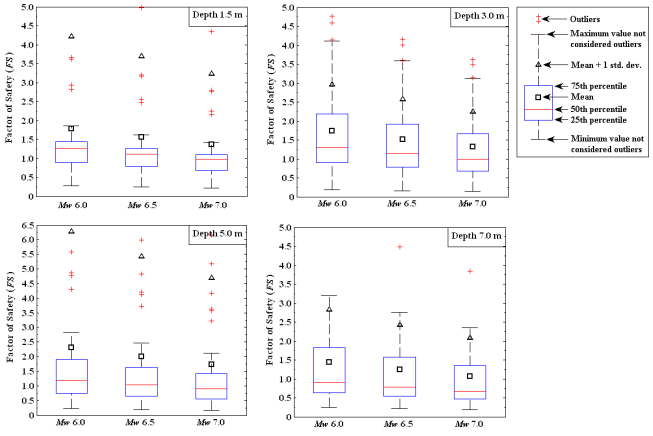

Fig. 5. Factors of safety against liquefaction (FS) for the city for earthquakes of 2475-yr return period.

3.2 Determination of cyclic resistance ratio

Determination of cyclic resistance ratio (CRR) requires fines content (FC) of the soil to correct updated SPT blow count $(N_1)_{60}$ to an equivalent clean sand standard penetration resistance value $(N_1)_{60cs}$. Idriss and Boulanger (2006) determined CRR value for cohesionless soil with any fines content using the following expression:

$$\mathrm{CRR} = \exp\left\{\frac{(N_1)_{60cs}}{14.1} + \left(\frac{(N_1)_{60cs}}{126}\right)^2 - \left(\frac{(N_1)_{60cs}}{23.6}\right)^3 + \left(\frac{(N_1)_{60cs}}{25.4}\right)^4 - 2.8\right\} \quad (12)$$

$$(N_1)_{60cs} = (N_1)_{60} + \Delta(N_1)_{60} \quad (13)$$

where $\Delta(N_1)_{60}$ is the correction for fines content in percent (FC) present in the soil and is expressed as

$$\Delta(N_1)_{60} = \exp\left(1.63 + \frac{9.7}{\mathrm{FC}+0.1} - \left(\frac{15.7}{\mathrm{FC}+0.1}\right)^2\right). \quad (14)$$

3.3 Determination of factor of safety

The factor of safety against liquefaction (FS) is commonly used to quantify liquefaction potential. The factor of safety against liquefaction (FS) can be defined by

$$\mathrm{FS} = \frac{(\mathrm{CRR})_{M_w=7.5}}{(\mathrm{CSR})_{M_w=7.5},\sigma'_v=1}\mathrm{MSF}. \quad (15)$$

Both CSR and CRR vary with depth, and therefore the liquefaction potential is evaluated at corresponding depths within the soil profile.

3.4 Determination of liquefaction potential index

Liquefaction potential index (LPI) is a single-valued parameter to evaluate regional liquefaction potential. LPI at a site is computed by integrating the factors of safety (FS) along the soil column up to 20 m depth. A weighting function is added to give more weight to the layers closer to the ground surface. The liquefaction potential index (LPI) proposed by Iwasaki et al. (1978, 1982) is expressed as follows:

$$\mathrm{LPI} = \int_0^{20} F(z).w(z)\mathrm{d}z \quad (16)$$

where z is depth of the midpoint of the soil layer (0 to 20 m) and dz is differential increment of depth. The weighting factor, $w(z)$, and the severity factor, $F(z)$, are calculated as per the following expressions:

$$F(z) = 1 - \mathrm{FS} \text{ for } \mathrm{FS} < 1.0 \quad (17)$$

$$F(z) = 0 \text{ for } \mathrm{FS} \geq 1.0 \quad (18)$$

$$w(z) = 10 - 0.5z \text{ for } z < 20\,\mathrm{m} \quad (19)$$

$$w(z) = 0 \text{ for } z > 20\,\mathrm{m} \quad (20)$$

For the soil profiles with the depth less than 20 m, LPI is calculated using the following expression (Luna and Frost 1998):

$$\mathrm{LPI} = \sum_{i=1}^{n} w_i F_i H_i \quad (21)$$

with

$$F_i = 1 - \mathrm{FS}_i \text{ for } \mathrm{FS}_i < 1.0 \quad (22)$$

$$F_i = 0 \text{ for } \mathrm{FS}_i \geq 1.0 \quad (23)$$

where H_i is thickness of the discretized soil layers; n is number of layers; F_i is liquefaction severity for i-th layer; FS_i is the factor of safety for i-th layer; w_i is the weighting factor ($= 10–0.5\,z_i$); and z_i is the depth of i-th layer (m).

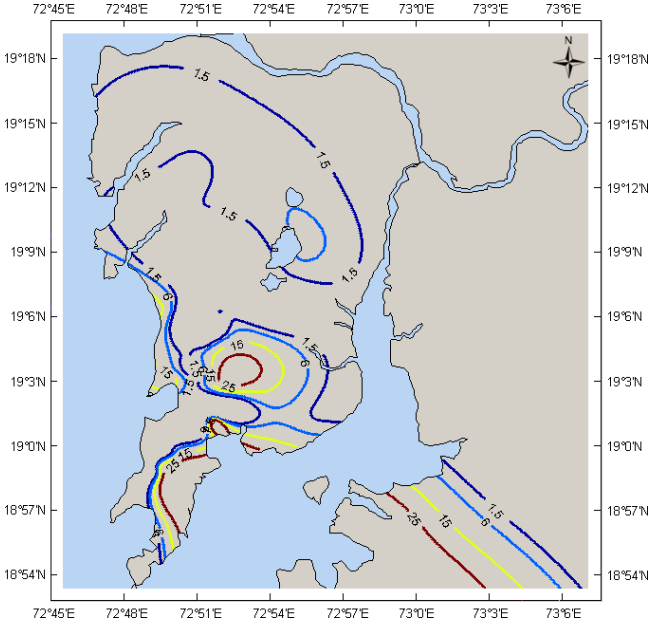

Fig. 6. Contour map of liquefaction potential index (LPI) for earthquake of magnitude $M_w = 6.0$ of 2475-yr return period.

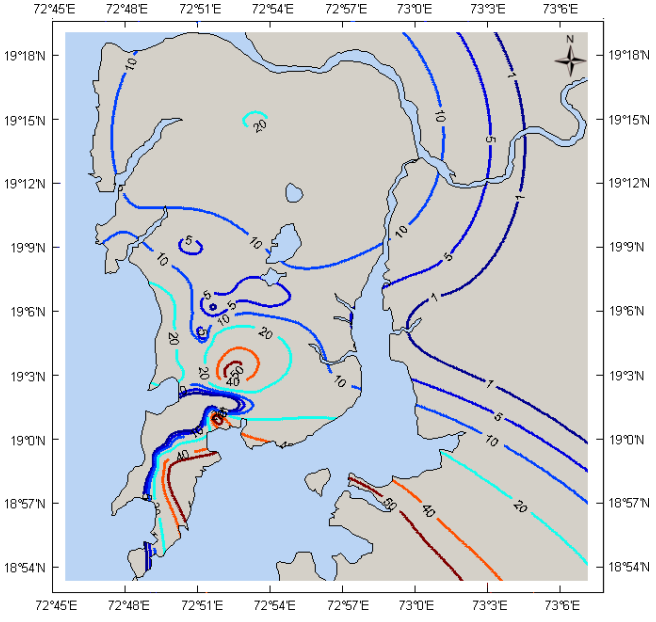

Fig. 8. Contour map of liquefaction potential index (LPI) for earthquake of magnitude $M_w = 7.0$ of 2475-yr return period.

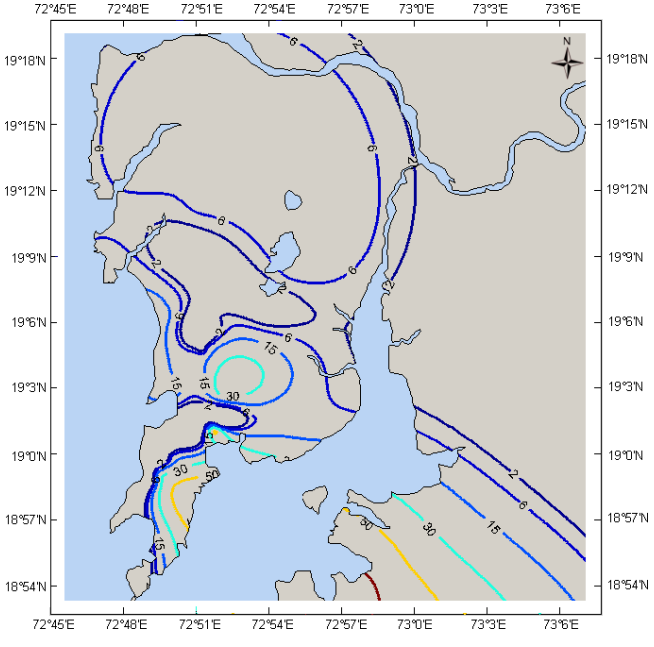

Fig. 7. Contour map of liquefaction potential index (LPI) for earthquake of magnitude $M_w = 6.5$ of 2475-yr return period.

3.5 Computation of liquefaction potential index at a typical site

A typical site has been chosen near Mahim as shown through encircled * in Fig. 1. The details of subsurface soil condition and SPT N profile are shown in Fig. 4. The soil deposit at this site comprises layers of fill, clayey sand, soft clay, stiff clayey silt, and very stiff clayey silt. The typical computation of factors of safety against liquefaction for earthquakes of different magnitudes is carried out at this chosen borehole using Eqs. (2) through (15). Earthquake magnitudes and a_{max} level used in the present study are as per the recommendations of Raghukanth and Iyengar (2006). Factors of safety (FS) at different depths of the soil profiles are computed for the earthquakes of magnitude $M_w = 6.0$, $M_w = 6.5$, and $M_w = 7.0$ with a_{max} value of 0.3 g. Figure 4 shows the soil profile, corrected N values, fines content, and FS values against liquefaction along the depth. LPI at this particular site is calculated from FS values based on the expressions by Luna and Frost (1998). LPI values are computed at the typical site for magnitudes of $M_w = 6.0$, $M_w = 6.5$, and $M_w = 7.0$, with a_{max} 0.3 g, and the results are presented in Tables 3 through 5. LPI values at this site show different levels of liquefaction severity depending on magnitudes of earthquake.

4 Results and conclusions

Considering the high importance of Mumbai city, this study attempts to evaluate the factors of safety against liquefaction (FS) and corresponding liquefaction potential indices (LPI) for the worst seismic scenario for the city using SPT-based semiempirical procedure. The FS values for the city are shown as box plots in Fig. 5. This figure graphically depicts all fundamental sets of descriptive statistics in a convenient way. These box plots present first quartile (25th percentile), medians, third quartile (75th percentile), mean, mean incremented by 1 standard deviation (SD), outliers,

Table 3. Computation of LPI for PGA 0.3 g corresponding to $M_w = 6.0$.

Depth (m)	Unit Wt. (kN m^{-3})	r_d	MSF	FC (%)	$(N_1)_{60cs}$	CSR	CRR	FS	z (m)	H (m)	$w(z)$	F	$w(z).F.H$
1.5	15	0.99	1.48	32	10.7	0.142	0.123	0.87	0.75	1.5	9.625	0.13	1.91
2.2	15	0.97	1.48	69	15.1	0.175	0.157	0.90	1.85	0.7	9.075	0.10	0.65
3.1	15.8	0.96	1.48	69	17.3	0.201	0.176	0.88	2.65	0.9	8.675	0.12	0.97
4.4	15.8	0.93	1.48	69	19.8	0.222	0.204	0.92	3.75	1.3	8.125	0.08	0.89
6	16	0.90	1.48	69	21.6	0.233	0.228	0.98	5.2	1.6	7.4	0.02	0.26
7.2	16	0.87	1.48	69	20.7	0.235	0.214	0.91	6.6	1.2	6.7	0.09	0.72
												LPI = $\Sigma w(z).F.H$	5.4

Table 4. Computation of LPI for PGA 0.3 g corresponding to $M_w = 6.5$.

Depth (m)	Unit Wt. (kN m^{-3})	r_d	MSF	FC (%)	$(N_1)_{60cs}$	CSR	CRR	FS	z (m)	H (m)	$w(z)$	F	$w(z).F.H$
1.5	15	0.99	1.30	32	10.7	0.162	0.123	0.76	0.75	1.5	9.625	0.24	3.48
2.2	15	0.98	1.30	69	15.1	0.200	0.157	0.78	1.85	0.7	9.075	0.22	1.37
3.1	15.8	0.97	1.30	69	17.3	0.231	0.176	0.76	2.65	0.9	8.675	0.24	1.85
4.4	15.8	0.94	1.30	69	19.8	0.257	0.204	0.79	3.75	1.3	8.125	0.21	2.18
6	16	0.91	1.30	69	21.6	0.271	0.228	0.84	5.2	1.6	7.4	0.16	1.87
7.2	16	0.89	1.30	69	20.7	0.274	0.214	0.78	6.6	1.2	6.7	0.22	1.77
												LPI = $\Sigma w(z).F.H$	12.5

minimum and maximum values of FS not included in outliers. The first quartile (Q_1) and third quartile (Q_3) are shown by the bottom and top of the rectangular box, respectively. The interquartile range (i.e. Q_3–Q_1) defines the size of the rectangle. A dataset can be easily described by a box plot without listing all the data, and the spread of distribution of the dataset can be easily sensed from these parameters. The median is shown by the red line near the middle of the box. The whiskers connect to the maximum and minimum FS values to the box. FS values that are more than one and a half times the length of one interquartile range of the box are called outliers, and these outliers are displayed separately as red-coloured addition symbols (+). Depending upon the dataset, they can be either positive or negative, or both. Figure 5 shows only positive outliers, as all FS values in the dataset are positive. The outliers are truncated in these box plots to enhance the clarity of presentation. The inset in Figure 5 describes all the notations used to signify the statistical parameters. Mean and mean+1SD are shown as squares (□) and triangles (△), respectively. FS values are much larger than 1 at many borehole locations in the city, and therefore the standard deviation value is reasonably large. The median is independent of the shape of the distribution of data values, and it is more resistant to the outliers than mean, though mean is more useful. The representation of mean is better for symmetrical distributions and of median is very appropriate for skewed distributions. FS value less than 1 at certain depth indicates that the soil layer at that particular depth is likely to liquefy. Mean and median FS values for a particular depth can be seen to be decreasing with increase in the magnitude of earthquake. This shows the increase in liquefaction vulnerability with increase in intensity of seismic events.

Seismic soil liquefaction potential in terms of LPI is determined at 142 sites across Mumbai city, and the contour maps of LPI values are generated for the city to show the spatial distribution of liquefaction potential. These LPI contour maps could give an indication of geographic variability of liquefaction effects and different kinds of probable surface manifestations of liquefaction. Spatial distribution of soil liquefaction potential for earthquakes of 2 % probability of exceedance is quantitatively presented in the form of contour maps showing the liquefaction potential index (LPI). Contour maps of LPI are generated for the city to predict the occurrence of damaging liquefaction for the earthquakes of magnitude $M_w = 6.0$, $M_w = 6.5$, and $M_w = 7.0$ of a_{max} level 0.3 g corresponding to 2475-yr return period and are shown in Figs. 6 through 8, respectively. These contour maps show the liquefaction vulnerability at different sites in the city. Liquefaction susceptibility for sites with LPI > 15 is very high, and the liquefaction is very unlikely at sites with LPI < 5. Some of the sites in the city: namely Sion, Wadala, Sewree, and Marine line, are highly vulnerable to severe liquefaction for $M_w = 6.0$ and a_{max} value of 0.3 g. LPI is greater than 15 for $M_w = 7.0$ and a_{max} value of 0.3 g at many sites in the city, namely Mahim, Wadala, Sion, Sewree, Trombay, JNPT, Goregaon, Bandra, Andheri, and Marine line.

Table 5. Computation of LPI for PGA 0.3 g corresponding to $M_w = 7.0$.

Depth (m)	Unit Wt. (kN m^{-3})	r_d	MSF	FC (%)	$(N_1)_{60cs}$	CSR	CRR	FS	z (m)	H (m)	$w(z)$	F	$w(z).F.H$
1.5	15	0.99	1.14	32	10.7	0.186	0.123	0.66	0.75	1.5	9.625	0.34	4.85
2.2	15	0.98	1.14	69	15.1	0.230	0.157	0.68	1.85	0.7	9.075	0.32	2.00
3.1	15.8	0.97	1.14	69	17.3	0.266	0.176	0.66	2.65	0.9	8.675	0.34	2.62
4.4	15.8	0.96	1.14	69	19.8	0.296	0.204	0.69	3.75	1.3	8.125	0.31	3.30
6	16	0.93	1.14	69	21.6	0.314	0.228	0.72	5.2	1.6	7.4	0.28	3.26
7.2	16	0.91	1.14	69	20.7	0.321	0.214	0.67	6.6	1.2	6.7	0.33	2.67
												LPI = $\Sigma w(z).F.H$	18.7

The areas developed on reclaimed land having large thickness of soft soil deposit and shallow ground water levels are observed to be more susceptible to liquefaction. This study reveals that the higher susceptibility of liquefaction at some of the places can be attributed to the higher thickness of soft soil deposits and ground water table at shallow depths. It can be observed from the LPI contour maps that a high degree of liquefaction damages is likely to occur at many sites in the city during severe seismic event. These LPI contour maps will help the structural designers and city planners to check the vulnerability of the area against liquefaction. These contour maps can also be used effectively for seismic safety plans and in the seismic hazard mitigation programs.

Acknowledgements. The authors extend their thanks to M/S DBM Geotechnics and Constructions Pvt Ltd., Mumbai for providing the borehole data at different sites in the study area.

Edited by: M. E. Contadakis
Reviewed by: N. Klimis and another anonymous referee

References

Boatwright, J., Seekins, L., Fumal, T. E., Liu, H. P., and Mueller, C. S.: Ground motion amplification in the Marina district, B. Seismol. Soc. Am., 81, 1980–1997, 1991.

Chandra, U.: Earthquakes of Peninsular India – A seismotectonic study, B. Seismol. Soc. Am., 67, 1387–1413, 1977.

Dixit, J., Dewaikar, D. M., and Jangid, R. S.: Spatial distribution of surface level free field motion at Mumbai city, Electronic J. Geotech. Eng., 16F, 661–677, 2011.

Dixit, J., Dewaikar, D. M., and Jangid, R. S.: Soil liquefaction studies at Mumbai city, Nat. Hazards, 63, 375–390, 2012.

Geological Survey of India (GSI): District Resource Map, Mumbai District, Maharashtra, 2001.

Holzer, T. L., Bennett, M. J., Noce, T. E., Padovani, A. C., and Tinsley, J. C.: Liquefaction hazard mapping with LPI in the Greater Oakland, California, area, Earthq. Spectra, 22, 693–708, 2006.

Hough, S. E., Martin, S., Bilham, R., and Atkinson, G. M.: The 26 January 2001 M 7.6 Bhuj, India. Earthquake: observed and predicted ground motion, B. Seismol. Soc. Am., 92, 2061–2079, 2002.

Idriss, I. M. and Boulanger, R. W.: Semi-empirical procedures for evaluating liquefaction potential during earthquakes, Soil Dynam. Earthq. Eng., 26, 115–130, 2006.

İnce, G. Ç.: The relationship between the performance of soil conditions and damage following an earthquake: a case study in Istanbul, Turkey, Nat. Hazards Earth Syst. Sci., 11, 1745–1758, doi:10.5194/nhess-11-1745-2011, 2011.

IS 1893 (part 1): Criteria for Earthquake Resistant Design of Structure, Bureau of Indian Standards, New Delhi, India, 2002.

Ishihara, K.: Stability of natural deposits during earthquakes, Proceedings of 11th International Conference on Soil Mechanics and Foundation Engineering, San Francisco, CA, 1, 321–376, 1985.

Iwasaki, T., Tokida, K., Tatsuko, F., and Yasuda, S.: A practical method for assessing soil liquefaction potential based on case studies at various sites in Japan, Proceedings of 2nd International Conference on Microzonation, San Francisco, 885–896, 1978.

Iwasaki, T., Tokida, K., Tatsuoka, F., Watanabe, S., Yasuda, S., and Sato, H.: Microzonation for soil liquefaction potential using simplified methods, Proceedings of 2nd International Conference on Microzonation, Seattle, 1319–1330, 1982.

Juang, C. H., Yuan, H., Li, D. K., Yang, S. H., and Christopher, R. A.: Estimating severity of liquefaction-induced damage near foundation, Soil Dynam. Earthq. Eng., 25, 403–411, 2005.

Kramer, S. L.: Geotechnical Earthquake Engineering, Prentice Hall, New Jersey, 1996.

Luna, R. and Frost, J. D.: Spatial liquefaction analysis system, J. Comput. Civil Eng., 12, 48–56, 1998.

Martin, S. and Szeliga, W.: A Catalog of Felt Intensity Data for 570 Earthquakes in India from 1636 to 2009, B. Seismol. Soc. Am., 100, 562–569, 2010.

Mhaske, S. Y. and Choudhury, D.: GIS-based soil liquefaction susceptibility map of Mumbai city for earthquake events, J. Appl. Geophys., 70, 216–225, 2010.

Microzonation for Earthquake Risk Mitigation (MERM): Microzonation Manual, World Institute for Disaster Risk Management, 2003.

Mohan, G., Surve, G., and Tiwari, P.: Seismic evidences of faulting beneath the Panvel flexure, Current Sci., 93, 991–996, 2007.

National Earthquake Hazards Reduction Program (NEHRP): Recommended Provisions for Seismic Regulations for New Buildings and Other Structures, FEMA P-750, Building Seismic Safety Council, Federal Emergency Management Agency, Washington DC, 2009.

Raghukanth, S. T. G.: Seismicity parameters for important urban agglomerations in India, Bull. Earthq. Eng., 9, 1361–1386, 2011.

Raghukanth, S. T. G. and Iyengar, R. N.: Seismic hazard estimation for Mumbai city, Current Sci., 91, 1486–1494, 2006.

Seed, H. B. and Idriss, I. M.: Simplified procedure for evaluating soil liquefaction potential, J. Soil Mech. Foundation Division, 97, 1249–1273, 1971.

Seed, H. B. and Idriss, I. M.: Ground motions and soil liquefaction during earthquakes, monograph, Earthquake Engineering Research Institute, Berkeley, CA, 1982.

Seed, H. B., Tokimatsu, K., Harder, L. F., and Chung, R.: Influence of SPT procedures in soil liquefaction resistance evaluations, J. Geotech. Eng. Division, 111, 1425–1445, 1985.

Sethna, S. F.: Geology around Bombay – some intriguing problems, Proc. Deccan Volcanism and Related Basalt Provinces in other Parts of the World, Geol. Soc. India, 3, 87–92, 1981.

Sethna, S. F.: Geology of Mumbai and surrounding areas and its position in the Deccan traps stratigraphy, J. Geol. Soc. India, 53, 359–365, 1999.

Sethna, S. F. and Battiwala, H. K.: Major element geochemistry of the intermediate and acidic rocks associated with the Deccan Trap basalts, Proc. 3rd Indian Geological Congress, Pune, 281–294, 1980.

Shah, S. D. and Parthasarathy, A.: Engineering geological studies of Bombay metropolitan region – their significance in the developmental aspects of the area, Proc. 4th Congress, International Association for Engineering Geology and the Environment, New Delhi, 1, 177–185, 1982.

Sonmez, H.: Modification of the liquefaction potential index and liquefaction susceptibility mapping for a liquefaction-prone area (Inegol, Turkey), Environ. Geol., 44, 862–871, 2003.

Subrahmanyan, V.: Seismic signatures in the Kalu River Basin, Thane district and Mumbai, in: Research Highlights in Earth System Science, Indian Geological Congress, 201–204, 2001.

Toprak, S. and Holzer, T. L.: Liquefaction potential index: Field assessment, J. Geotech. Geoenviron. Eng., 129, 315–322, 2003.

Tuttle, M., Chester, J., Lafferty, R., Dyer-Williams, K., and Cande, B.: Paleoseismology study northwest of the New Madrid Seismic Zone, US Nuclear Regulatory Commission, NUREG/CR-5730, Washington, DC, 1999.

Ulusay, R. and Kuru, T.: 1998 Adana-Ceyhan (Turkey) earthquake and a preliminary microzonation based on liquefaction potential for Ceyhan Town, Nat. Hazards, 32, 59–88, 2004.

Youd, T. L. and Perkins, D. M.: Mapping liquefaction-induced ground failure potential, J. Geotech. Eng. Division, 104, 443–446, 1978.

Youd, T. L., Idriss, I. M., Andrus, R. D., Arango, I., Castro, G., Christian, J. T., Dobry, R., Finn, W. D. L., Harder Jr., L. F., Hynes, M. E., Ishihara, K., Koester, J. P., Liao, S. S. C., MarcusonIII, W. F., Martin, G. R., Mitchell, J. K., Moriwaki, Y., Power, M. S., Robertson, P. K., Seed, R. B., and Stokoe II, K. H.: Liquefaction resistance of soils summary report from 1996 NCEER and 1998 NCEER/NSF workshops on Evaluation of Liquefaction Resistance of Soil, J. Geotech. Geoenviron. Eng., 127, 817–833, 2001.